Mechanisms of protease-activated receptor 2-evoked hyperexcitability of nociceptive neurons innervating the mouse colon

Mechanisms of protease-activated receptor 2-evoked hyperexcitability of nociceptive neurons innervating the mouse colon

Ahmed Kayssi[1], Silvia Amadesi[2], Francisco Bautista[1], Nigel W. Bunnett[2] and Stephen Vanner[1]

[1]*Gastrointestinal Diseases Research Unit, Queen's University, Kingston, Ontario, Canada*
[2]*Departments of Surgery and Physiology, University of California, San Francisco, CA, USA*

Agonists of protease-activated receptor 2 (PAR_2) evoke hyperexcitability of dorsal root ganglia (DRG) neurons by unknown mechanisms. We examined the cellular mechanisms underlying PAR_2-evoked hyperexcitability of mouse colonic DRG neurons to determine their potential role in pain syndromes such as visceral hyperalgesia. Colonic DRG neurons were identified by injecting Fast Blue and DiI retrograde tracers into the mouse colon. Using immunofluorescence, we found that DiI-labelled neurons contained PAR_2 immunoreactivity, confirming the presence of receptors on colonic neurons. Whole-cell current-clamp recordings of acutely dissociated neurons demonstrated that PAR_2 activation with a brief application (3 min) of PAR_2 agonists, SLIGRL-NH_2 and trypsin, evoked sustained depolarizations (up to 60 min) which were associated with increased input resistance and a marked reduction in rheobase (50% at 30 min). In voltage clamp, SLIGRL-NH_2 markedly suppressed delayed rectifier I_K currents (55% at 10 min), but had no effect on the transient I_A current or TTX-resistant Na^+ currents. In whole-cell current-clamp recordings, the sustained excitability evoked by PAR_2 activation was blocked by the PKC inhibitor, calphostin, and the $ERK_{1/2}$ inhibitor PD98059. Studies of $ERK_{1/2}$ phosphorylation using confocal microscopy demonstrated that SLIGRL-NH_2 increased levels of immunoreactive $pERK_{1/2}$ in DRG neurons, particularly in proximity to the plasma membrane. Thus, activation of PAR_2 receptors on colonic nociceptive neurons causes sustained hyperexcitability that is related, at least in part, to suppression of delayed rectifier I_K currents. Both PKC and $ERK_{1/2}$ mediate the PAR_2-induced hyperexcitability. These studies describe a novel mechanism of sensitization of colonic nociceptive neurons that may be implicated in conditions of visceral hyperalgesia such as irritable bowel syndrome.

(Resubmitted 13 December 2006; accepted after revision 6 February 2007; first published online 8 February 2007)
Corresponding author S. Vanner: Hotel Dieu Hospital, 166 Brock Street, Kingston, Ontario, Canada K7L 5G2. Email: vanners@hdh.kari.net

The irritable bowel syndrome (IBS) is a common disorder affecting daily living and quality of life (Lembo *et al.* 2005). Of those symptoms that characterize IBS (i.e. abdominal pain, altered bowel pattern such as constipation and diarrhoea, abdominal bloating and altered defecation), abdominal pain is reported to be most troublesome and best correlates with severity of illness (Sandler *et al.* 1984). The lack of available therapies to effectively manage this pain continues to stimulate studies of the mechanisms that underlie this pain and to define novel therapeutic targets.

Visceral hypersensitivity (i.e. an increased sensitivity to stimuli arising from the intestinal wall) is widely recognized to underlie abdominal pain in IBS, at least in a significant subset of patients (gado-Aros & Camilleri, 2005). Both central and peripheral mechanisms have been implicated and their relative role may be dependent on the clinical setting. In the periphery, sensitization of nociceptive nerve endings in the wall of the colon appears to be important. This may result from signalling from low levels of persisting cytokines in conditions such as post-infectious IBS (Spiller & Campbell, 2006), although there is also growing evidence that release of mast cell mediators may contribute to peripheral sensitization in IBS (Barbara *et al.* 2004).

Of the many substances released from mast cells, proteases such as tryptase may play a particularly important role in signalling to neurons (Barbara *et al.* 2004; Spiller & Campbell, 2006). The number of tryptase-containing mast cells is increased in intestinal tissues of patients with IBS (Barbara *et al.* 2004; 2006).

 DOI: 10.1113/jphysiol.2006.126599

Moreover, tryptase levels in tissues, and tryptase release from biopsies are increased in IBS patients (Barbara *et al.* 2004). Proteases such as tryptase can signal to enteric (Reed *et al.* 2003) and dorsal root ganglia (DRG) (Vergnolle *et al.* 2001) neurons by cleaving and activating protease-activated receptors (PARs) to induce sustained increases in their excitability. While hyperexcitability of enteric neurons could result in disturbances in intestinal secretion and motility, hyperexcitability of DRG neurons could be an important mechanism of peripheral sensitization in conditions such as IBS (Mawe *et al.* 2004; Beyak & Vanner, 2005; Lomax *et al.* 2006). Although whole-animal studies have demonstrated a role for mast cell proteases signalling to PARs in the genesis of visceral hypersensitivity (Vergnolle *et al.* 2001), the precise mechanism(s) by which this occurs remain unclear.

Certain serine proteases that are generated and released during inflammation can signal to cells by cleaving protease-activated receptors (PARs), a family of four G-protein-coupled receptors. Cleavage exposes a tethered ligand domain that binds to and activates the cleaved receptors. Synthetic peptides that correspond to the tethered ligand domain of PAR_1, PAR_2, and PAR_4 directly activate these receptors and are useful tools to probe receptor function. Of the four cloned PARs, tryptase selectively activates PAR_2, and trypsins are also potent activators of this receptor (Saito & Bunnett, 2005). PAR_2 is expressed by DRG and enteric neurons, and PAR_2-selective activating peptides induce hyperexcitability of these neurons. Although the digestive tract is the richest source of proteases that can activate PAR_2, such as tryptase and trypsins, the effect of PAR_2 agonists on hyperexcitability of colonic nociceptive DRG neurons has not been examined. Moreover, although PAR_2 agonists are known to cause hyperexcitability of DRG neurons (Amadesi *et al.* 2004), the mechanisms of this effect are unknown. In the present study we examined the effects of PAR_2 activation with a selective agonist on the neuronal excitability of mouse colonic DRG nociceptive neurons. Our aims were to (1) determine if colonic DRG neurons express immunoreactive PAR_2, using retrograde tracing and immunofluorescence; (2) examine whether activation of PAR_2 results in hyperexcitability of these neurons, and to identify any effects upon voltage-gated potassium or sodium currents using electrophysiological approaches; (3) identify the kinases that mediate PAR_2-induced hyperexcitability using pharmacological approaches; and (4) determine if activated kinases are appropriately localized to regulate the affected ion channels, using immunofluorescence and confocal microscopy. Small DRG neurons were studied because these neurons express properties associated with nociceptors (Gold *et al.* 1996*a*; Yoshimura & de Groat, 1999; Moore *et al.* 2002; Beyak & Vanner, 2005). We found that PAR_2 activation evoked a sustained hyperexcitability of these colonic neurons, and sought to determine the mechanism(s) that underlies this action.

Methods

Drugs and reagents

Synthetic peptides corresponding to the tethered ligand of rat and mouse PAR_2 (PAR_2-activating peptide, PAR_2-AP, SLIGRL-NH_2) and the reverse peptide sequence that does not activate PAR_2 (PAR_2-reverse peptide, PAR_2-RP, LRGILS-NH_2, control) were from Sigma Genosys (The Woodlands, TX, USA). All other chemicals were obtained from Sigma, with the exception of TTX and PD98059 (Calbiochem). All agonists were applied to the bath using a fast-flow solution-switching system (VC6; Warner Instruments) and a three-barrel square glass (Harvard Apparatus). In electrophysiological studies involving PD98059, the cells were incubated with the drugs for a minimum of 2 h before the experiment began. Both PD98059 and calphostin C were included in the bath and pipette solutions.

Animals

Electrophysiological studies were conducted on CD-1 mice (Charles River Laboratories, Montreal, QC, Canada) of either sex, weighing 30–40 g. Immunohistochemical studies were conducted on C57Bl6 mice (6–8 weeks) from Jackson Laboratories (Bar Harbour, ME, USA) and Sprague-Dawley rats (male, 200–250 g) from Charles River Laboratories (Wilmington, MA, USA). The Queen's University Animal Care Committee and the UCSF Institutional Animal Care and Use Committees approved and monitored all procedures with these animals. At the end of experiments, animals were killed using sodium pentobarbitone (200 mg kg^{-1}, I.P.) and bilateral thoracotomy.

Retrograde labelling of colonic neurons

Mice or rats were anaesthetized with isoflurane (5%) or a combination of ketamine hydrochloride (Pfizer; New York, NY, USA) 18.75 mg ml^{-1} and xylazine (Bayer; Etobicoke, ON, USA) 1.25 mg ml^{-1} injected I.P. (0.1 ml (10 g body weight)$^{-1}$). The descending colon was exposed by a midline laparotomy. A 25 μl syringe (Hamilton, Reno, Nevada, USA) with a 30–32 gauge needle was used to inject Fast Blue (17 mg ml^{-1}, volume = 1.0 μl per injection) or 1,1-dioctadecyl-3–3-3′3′-tetramethylindocarbocyanine (DiI) (5–17 mg ml^{-1} in DMSO) into 5–10 sites along the colon wall (volume = 10 μl per injection site), as previously described (Beyak *et al.* 2004). Excess dye was removed using a cotton swab to prevent the dye leaking to other tissues. The abdomen was irrigated with saline and sutured closed. After surgery, animals were allowed to recover on a warming blanket and were given free

access to water and food. After recovery from anaesthesia, animals were monitored for signs of pain, feeding, and weight loss. Animals that displayed behaviour consistent with ongoing pain or failure to thrive were killed.

Immunohistochemical localization of PAR_2

Ten to fifteen days following DiI injection, animals were killed using sodium pentobarbital (200 mg kg^{-1} I.P.). DRG (T9–L1, T5 for control) were immersion fixed in 4% paraformaldehyde in 100 mM PBS pH 7.4 for 4 h at 4°C, washed with PBS and placed in a 25% sucrose solution overnight at 4°C. DRG were embedded in OCT compound (Miles, Elkhart, IN, USA) and sectioned at 25 μm. Sections were washed in PBS containing 1–10% NGS, 1% BSA and 0.3–0.5% Triton X-100, and incubated with primary antibodies to PAR_2 (mouse DRG, A5, 1 : 750; rat DRG, SAM11, 1 : 250) overnight at 4°C. Sections were washed and incubated with goat anti-antirabbit or antimouse IgG conjugated to FITC (1 : 200, room temperature, 2 h). Sections were washed and mounted in Prolong (Molecular Probes, Eugene, OR, USA). Mouse monoclonal antibodies to PAR_2 (SAM11) were from Santa Cruz Biotechnology (Santa Cruz, CA, USA). Rabbit antibody to PAR_2 (A5) was from Dr M. Hollenberg (Calgary University). Goat antimouse or antirabbit IgG conjugated to FITC was from Jackson ImmunoResearch (West Grove, PA, USA).

Isolation and culture of DRG neurons for ERK phosphorylation studies

Mice and rats were killed using sodium pentobarbital (200 mg kg^{-1} I.P.). DRG from thoracic and lumbar spinal cord were minced in cold Hank's balance salt solution (HBSS) (Steinhoff *et al.* 2000; Amadesi *et al.* 2004). Mouse DRG were digested by incubating in DMEM containing 1 mg ml^{-1} collagenase type 1A and 0.8 mg ml^{-1} DNAse type IV, for 60 min at 37°C. This solution was removed and neurons were incubated for 45 min at 37°C with DMEM containing 0.25% trypsin. Rat DRG were digested by incubating in Dulbecco's modified Eagle's medium (DMEM) containing 0.5 mg ml^{-1} trypsin, 1 mg ml^{-1} collagenase type IA and 0.1 mg ml^{-1} DNAse type IV (all from Sigma, St Louis, MO, USA) for 60–90 min at 37°C. After digestion, soybean trypsin inhibitor (Sigma, 0.5%) was added to neutralize trypsin. Neurons were pelleted, suspended in DMEM containing 10% fetal bovine serum, 10% horse serum, 100 u ml^{-1} penicillin, 0.1 mg ml^{-1} streptomycin, 2 mM glutamine and 2.5 μg ml^{-1} DNAse type IV, plated on glass coverslips coated with Matrigel (BD Biosciences, Bedford, MA, USA), and cultured for 2–3 days.

ERK phosphorylation assays

Neurons in short-term culture (48–72 h) were incubated for 18 h at 37°C in DMEM containing 1% horse serum, 1% fetal bovine serum, 100 u ml^{-1} penicillin, 0.1 mg ml^{-1} streptomycin, 2 mM glutamine and 2.5 μg ml^{-1} DNAse IV. Neurons were washed and incubated for 30 min at 37°C in DMEM containing 0.1% BSA (protease-free). Neurons were challenged by addition of SLIGRL-NH_2 (PAR_2-AP) or LRGILS-NH_2 (PAR_2-RP) (both 100 μM) or PMA (1 μM) for 0–30 min. Neurons were immediately washed in ice-cold PBS (100 mM, pH 7.4), and were fixed in 4% paraformaldehyde in PBS for 20 min at room temperature. Neurons were incubated for 30 min at room temperature in PBS containing 1% NGS and 0.1% saponin, and were incubated overnight at 4°C with pERK antibody (1 : 500). Neurons were washed and incubated with goat antimouse IgG conjugated to FITC (1 : 200, room-temperature, 1 h). Slides were washed, fixed for 20 min in paraformaldehyde, and mounted in Vectashield with DAPI (Vector Laboratories, Burlingame, CA, USA). Mouse monoclonal antibodies to phosphorylated $ERK_{1/2}$ ($pERK_{1/2}$, E4) were from Santa Cruz Biotechnology (Santa Cruz, CA, USA).

Confocal microscopy

Specimens were observed using a Zeiss Axiovert microscope, a Bio-Rad MRC1000 confocal microscope, with a Zeiss Plan Apo ×40 (NA 1.4) objective for tissue sections and a Zeiss Plan Apo ×100 (NA 1.3) objective for cultured neurons. Images were collected at laser intensities of 3–30%, an iris of 2.5–3 mm and a zoom of 1–2, and typically 5–10 optical sections were taken at intervals of 0.5–1.0 μm. Images were processed to adjust contrast and brightness using Adobe Photoshop 7.0 (Adobe Systems, Mountain View, CA, USA). In experiments to localize $pERK_{1/2}$ in cultured neurons, images were collected under identical conditions (laser intensity, iris and gain) for control and stimulated neurons.

Electrophysiological studies

Neurons were acutely dissociated as previously described (Beyak *et al.* 2004). Briefly, tissue was incubated in collagenase (Worthington; Lakewood, NJ, USA) 1 mg ml^{-1} and dispase (Roche; Indianapolis, IN, USA) (4 mg ml^{-1}) for 10 min at 37°C, titurated with a fire-polished Pasteur pipette, and incubated for an additional 5 min at 37°C. Dissociated neurons were plated onto vitrogen-coated coverslips and stored in a humidified incubator at 37°C, under 95% air–5% CO_2 until retrieval (4–24 h) for electrophysiological studies. The incubating media was obtained from a stock solution containing 10 ml fetal bovine serum, 1 ml penicillin/streptomycin, 0.028 g glutamine, 0.6 g dextrose and 0.2 g $NaHCO_3$, and made up to 100 ml with DMEM (pH 7.2–7.3).

Whole-cell or perforated-patch-clamp electrophysiological experiments were performed in current or

voltage clamp at room temperature. Neurons adhering to the glass coverslip were placed in an RC-26 recording chamber (Warner Instruments; Hamden, CT, USA), which was mounted on the stage of an inverted microscope (Olympus IX70; Tokyo, Japan) fitted for both bright-field and fluorescence microscopy. With the use of the U-MWIG2 filter (Olympus) for Fast Blue, labelled colonic neurons were identified by their bright blue fluorescence. All cells were labelled with Fast Blue except in some latter experiments where a few unlabelled neurons were studied because of relatively lower numbers of labelled neurons. Almost all of these latter experimental groups had ∼50% or more labelled neurons, and no differences were observed between labelled and unlabelled neurons. Only small neurons ($\leq$25 μm diameter and $\leq$40 pF capacitance) were studied, because these neurons express properties associated with nociceptors (i.e. capsaicin sensitivity, TTX-resistant action potentials) (Gold *et al.* 1996*a*; Yoshimura & de Groat, 1999; Moore *et al.* 2002; Beyak & Vanner, 2005) Recordings were obtained using G85165T-4 patch glass capillary tubing with flame-polished ends (Warner Instruments), pulled with a PP-830 micropipette puller from Narishige (East Meadow, NY, USA), and fire-polished by using an FP-830 fire polisher (Narishige). Final pipette resistance was between 2 and 5 MΩ for all experiments. Signals were amplified using an Axopatch 200B amplifier and digitized with a Digidata 1322A A/D converter from Axon Instruments (San Jose, CA, USA). Signals were low-pass filtered at 5 kHz, acquired at 20 kHz, and stored on disk using Clampex 8.2 (Axon Instruments).

Data were only analysed from recordings that exhibited the following properties. The starting seal resistance between the cell membrane and the electrode tip was $\geq$1 GΩ. The starting series resistance was $\leq$20 MΩ, and remained stable throughout the experiment. In current clamp, cells had a stable resting membrane potential more negative than −45 mV for more than 5 min before recording, and displayed overshooting action potentials (peak $\geq$ +50 mV) for the duration of the experiment. In voltage clamp, the leak current was $\leq$0.5 nA when tested at a holding potential of −100 mV throughout the experiment. All perforated-patch recordings were obtained using amphotericin B from Sigma (St Louis, MO, USA) as previously described (Rae *et al.* 1991). Briefly, amphotericin B stock solution was made by diluting 6 mg of powder into 100 μl dimethylsulfoxide (DMSO) (Sigma), followed by sonication and vortex-mixing. Immediately prior to experiments, 20 μl of stock solution were added into 5 ml of internal pipette solution. The solution was vortexed until a uniform light-yellowish tint developed, then covered with aluminium foil to prevent exposure to light. The final amphotericin B concentration was 240 μg ml^{-1}. Due to the compound's photosensitivity and rate of breakdown upon exposure to light, pipette solutions with amphotericin B were replaced every 2 h. Pipette tips were dipped briefly into amphotericin-free internal pipette solution, then back-filled with unfiltered amphotericin-containing solution.

Current-clamp recordings were carried out in perforated-patch mode using the following solutions (mM): (pipette) 140 KCl, 10 Hepes, 5 EGTA, 4 Na_2-ATP, 5 $MgCl_2$, 2.5 $CaCl_2$ with pH adjusted to 7.2 using KOH; (bath), 140 NaCl, 5 KCl, 1 $MgCl_2$, 2 $CaCl_2$, 10 Hepes, and 10 D-glucose, with pH adjusted to 7.4 using NaOH.

The membrane potential was continuously monitored using Clampex 8.2. After a stable membrane potential was recorded for 5 min, membrane potential, rheobase, twice rheobase, and input resistance were recorded. Cells were then superfused with PAR_2-AP or PAR_2-RP (both 100 μM) for 3 min and the parameters were again measured at 3, 10, 30 and 60 min after application of the peptide. Rheobase was recorded using 180 ms steps in 0.01 nA increments, which continued until an action potential was fired and the current needed to generate the action potential was recorded. Input resistance was recorded using a single 180 ms hyperpolarizing step command equal to the negative value of the cell's rheobase, and varied between −0.1 and −0.3 nA. The membrane response to the PAR_2 agonist trypsin (300 nM) was tested in a separate series of experiments.

To record potassium currents, perforated patch was first established using the current-clamp bath solution described above. After perforation was complete, sodium-free bath solution was perfused onto the cell to isolate potassium currents. The composition (mM) was: 140 NMDG, 4 KCl, 1.8 Hepes, 1 D-glucose, 1 $CaCl_2$, 1 $MgCl_2$, pH adjusted to 7.4 using HCl. Pipette solution composition was (mM): 110 K-aspartate, 30 KCl, 10 EGTA, 10 Hepes, 2 Na_2-ATP, 1 $MgCl_2$, pH adjusted to 7.2 using KOH.

To study the effect of PAR_2 activation on I_A and I_K currents, neurons were superfused for 3 min with PAR_2-AP or PAR_2-RP (both 100 μM). I_A and I_K currents were separated using voltage protocols, as previously described (Stewart *et al.* 2003). Briefly, I_K was isolated using 400 ms depolarizing steps in 15 mV increments from −90 mV to +45 mV at a holding potential of −60 mV, with the sustained I_K measured isochronally, 400 ms after the onset of the pulse, at which time I_A was largely inactivated, minimizing contamination by this current. The I_A was isolated by subtracting the sustained I_K from the total potassium current recorded using 400 ms depolarizing steps in 15 mV increments from −90 mV to +45 mV from a holding potential of −100 mV. Peak I_A was measured as the peak of the transient component of this subtracted current. Recordings were made at the beginning of the experiment and at 3, 5, 10 and 15 min following the application of the peptide.

Voltage-clamp studies of Na^+ currents were carried out in whole-cell mode. All recordings were obtained with the

following solutions (mM): (pipette) 110 CsCl, 1 $MgCl_2$, 11 EGTA, 10 Hepes, 10 NaCl, pH adjusted to 7.2 with CsOH; (bath), 55 NaCl, 80 cholineCl, 2 $CaCl_2$, 1 $MgCl_2$, 10 Hepes, and 5 D-glucose, pH adjusted to 7.4 using NaOH. The low extracellular sodium concentration was used to reduce the size of the sodium currents, enabling them to be accurately clamped. Na^+ currents were recorded in voltage clamp using 30 ms depolarizing steps in 5 mV increments from −80 to +40 mV at a holding membrane potential of −100 mV. TTX-resistant Na^+ currents were isolated with TTX (1 μM). The PAR_2 agonist SLIGRL-NH_2 (100 μM) or LRGILS-NH_2 (100 μM) was then superfused for 3 min, and voltage protocols in the presence of TTX repeated at 3, 5, and 10 min following application of the peptide.

Conductance was determined using the relation:

$$G = I/(V_m - E_X)$$

where G is the conductance, I is the measured membrane current, V_m is the command voltage, and E_X is the equilibrium potential, which was calculated to be −84 mV for potassium and +89.82 mV for sodium in control solutions. Normalized average conductances were plotted against membrane potential and the resultant curve was fitted to a Boltzmann function of the form:

$$G/G_{max} = 1/(1 + \exp[V_{50} - V_m/k])$$

where G is the conductance, G_{max} is the fitted maximal conductance, V_{50} is the membrane potential for half-activation, V_m is the command potential, and k is the slope factor.

Inactivation curves were measured using a two-pulse protocol, as previously described (Yoshimura & de Groat, 1999; Stewart *et al.* 2003). I_A inactivation curve studies used a 1 s prepulse varying between −120 and 0 mV, followed by a 400 ms test pulse of +50 mV. I_K inactivation curves were generated using a two-pulse protocol: an 8 s prepulse varying between −80 and 0 mV, followed by a 1 s test pulse of +50 mV. TTX-R sodium current inactivation curves were generated using a two-pulse protocol: a 1 s prepulse between −120 and 0 mV, followed by a 30 ms test pulse to 0 mV. Residual current amplitudes were normalized and plotted against conditioning pulse potential, and the continuous line in Fig. 4*E* is an average of fits to a negative Boltzmann function:

$$I/I_{max} = 1/(1 + \exp[V_{50} - V_m/k]),$$

where I is the current, I_{max} is the maximal current, V_{50} is the membrane potential for half-activation, V_m is the command potential, and k is the slope factor.

Statistical analysis

Electrophysiological recordings were analysed using Clampfit 8.2 software (Axon Instruments). Linear leak subtraction was used for all experiments with the P/N Clampfit protocol. Values obtained at various time points were expressed as a difference (absolute or percentage) from the resting membrane potential at $t = 0$ min. Data are expressed as means ± S.E.M. A two-way analysis of variance (ANOVA) with a Bonferroni *post hoc* test for significance was carried out to compare the results at every time point, and data values were deemed statistically significant if $P < 0.05$. Data from Fast Blue and non-labelled cells were also compared at every time point and were always found to be statistically insignificant ($P > 0.05$). Fitting of data was done with the least squares method using the fit function in Prism 4.0 (Graphpad Software). Voltages of half-activation (V_{50}), time constants, and slope factors were obtained from means of the individual Boltzmann curve fits.

Results

PAR_2 is expressed in colonic neurons

We have previously reported that nociceptive neurons of rat DRG that express TRPV1, CGRP and SP also express PAR_2 (Steinhoff *et al.* 2000; Amadesi *et al.* 2004). To determine if those DRG neurons innervating the colon contain PAR_2, we used retrograde tracing. When the tracer DiI was injected into the distal colon of mice, labelled DRG neurons could be detected in DRG from T9–L1 after 10–15 days (Fig. 1*A*). These neurons expressed immunoreactive PAR_2 (Fig. 1*B* and *C*). Since we have previously reported that PAR_2 is expressed by nociceptive DRG neurons in rats, and because intracolonic administration of PAR_2 activators causes hyperalgesia to distension of the rat colon, we also determined if DRG neurons innervating the colon express PAR_2 in this species. When DiI was injected into the distal colon of rats, labelled DRG neurons were detected in DRG from T9–L1 after 10–15 days (Fig. 1*D*). These neurons expressed immunoreactive PAR_2 (Fig. 1*E* and *F*). Together, these results show that DRG neurons that innervate the distal colon of mice and rats express PAR_2.

PAR_2 activation on mouse colonic DRG neurons evokes sustained hyperexcitability

Current-clamp recordings were obtained from 64 DRG neurons. Only small neurons were chosen for study (cell diameter ≤25 μm and a capacitance ≤40 pF) because these small cells have been shown to have properties exhibited by nociceptors (Beyak & Vanner, 2005). The mean resting membrane potential was −51.6 ± 1.6 mV. The mean input resistance was 585.29 ± 65.80 MΩ. All action potentials obtained displayed a shoulder on the repolarizing phase of the action potential, characteristic of TTX-resistant action potentials on nociceptive DRG neurons (Beyak & Vanner,

2005). Fewer than 10% of cells displayed spontaneous action potentials.

We have previously shown that PAR_2 activation on guinea-pig submucosal (Reed *et al.* 2003) and rat DRG neurons (Amadesi *et al.* 2004) caused a sustained decrease in rheobase and in rat DRGs a prolonged membrane depolarization. To evaluate the effect of PAR_2 activation on mouse colonic DRG neurons, Fast Blue-labelled neurons were superfused for 3 min with the PAR_2-AP (100 μM) and changes in passive and active membrane properties were compared to baseline for 60 min. Superfusion of PAR_2-AP ($n = 5$) caused a significant membrane potential depolarization at 3 min (mean = 6.8 mV; range: 2.1–12.4 mV) in all neurons tested, which peaked by 10 min (mean = 7.8 mV; range: 2–15.2 mV) (Fig. 2). This depolarization, although smaller, was still evident at 60 min. In contrast, superfusion with the reverse peptide PAR_2-RP (100 μM; $n = 6$ Fast Blue-labelled) had no effect on membrane potential.

PAR_2-AP (100 μM) also caused a decrease in rheobase at 3 min (mean = 55.5%; range: 33.3–71.4%), which was maximal by 60 min (mean = 73.3%; range: 56.2–100%) (Fig. 3*B*). Changes in membrane potential were controlled for by manually applying DC current to return the membrane potential to the resting value at each time point before retesting the rheobase. PAR_2-RP had no effect on rheobase. Changes in input resistance were monitored with constant hyperpolarizing pulses (see trace in Fig. 2*A*). PAR_2 activation caused a significant increase in input resistance at 3 min (mean = 68.3%; range: 5.44–201.94%), which was maximal by 60 min (73.3%; range: 49.4–108%) (Fig. 3*C*). Conversely, the reverse peptide had no effect on input resistance. Most neurons fired one or two action potentials when depolarized at 2× rheobase. These numbers did not change following activation of PAR_2 receptors (data not shown).

In a separate series of experiments, the PAR_2-AP (1–100 μM) displayed a dose-dependent effect on membrane potential (Fig. 2*C*). Two out of eight neurons did not respond to 30 μM and 100 μM PAR_2-AP. Superfusion of the PAR_2 agonist trypsin (300 nM) also evoked slow depolarizations (mean peak amplitude = 3.8 ± 0.53 mV; $n = 7$).

The effects of PAR_2-AP on action potential duration and slope were also evaluated in a separate series of experiments, using short-duration depolarizing pulses (30 ms). Following PAR_2 activation, the mean action potential duration ($n = 4$) at one-half the peak amplitude (Fig. 3) was longer at all time points (3–15 min; $n = 6$) and statistically significant at 15 min (0 min mean = 3.18 ± 0.53 *versus* 15 min mean = 3.48 ± 0.50; $P < 0.05$, $n = 6$). The action potential duration was unchanged in control neurons ($n = 4$) over a similar time period (0 min mean = 2.49 ± 0.49 ms

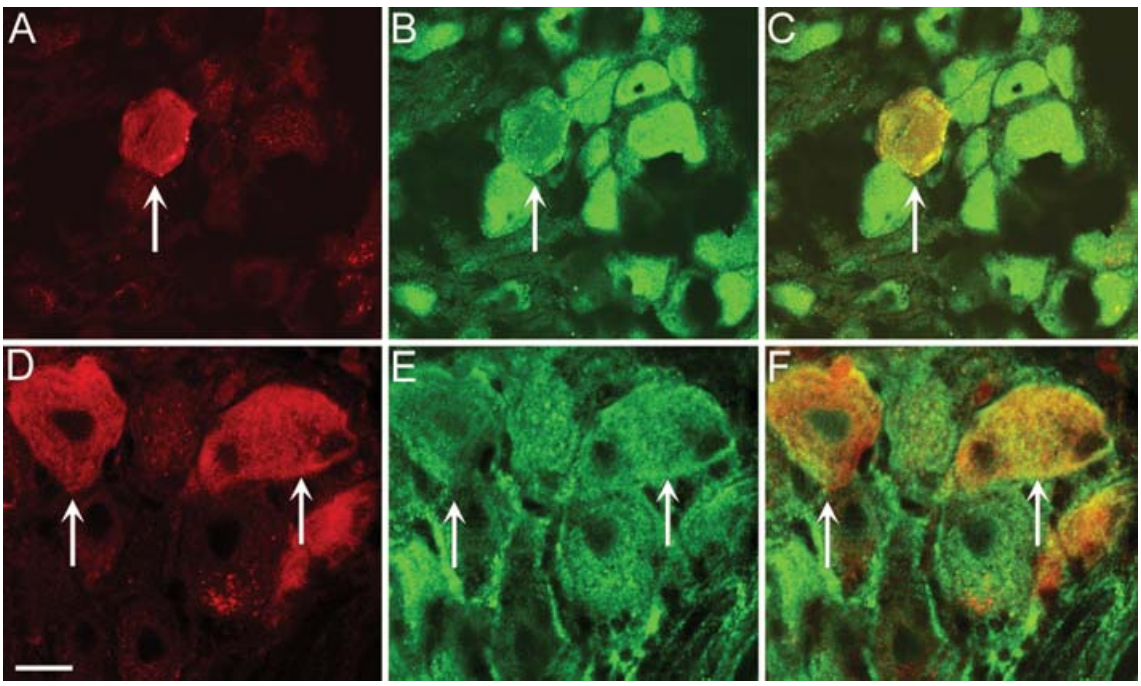

Figure 1. Localization of immunoreactive PAR_2 in retrogradely labelled DRG from mouse (*A–C*) and rat (*D–F*) DRG

DiI was injected into the wall of the distal colon and PAR_2 was localized in DRG (T9–L1) 10–15 days later. *A* and *D*, DiI; *B* and *E*, immunoreactive PAR; *C* and *F*, merge. DiI-labelled neurons innervating the colon expressed PAR_2 immunoreactivity. Representative images are shown from experiments on $n = 3$ animals. Scale bar = 20 μm. Arrows show labelled neuron.

versus 10 min mean = 2.49 ± 0.46 ms). The rising slope of the action potential was measured up to 10 min following PAR_2 activation ($n = 5$), and was not altered (0 min mean = 133.41 ± 11.43 mV ms^{-1} *versus* 0 min mean = 121.77 ± 17.63 mV ms^{-1}).

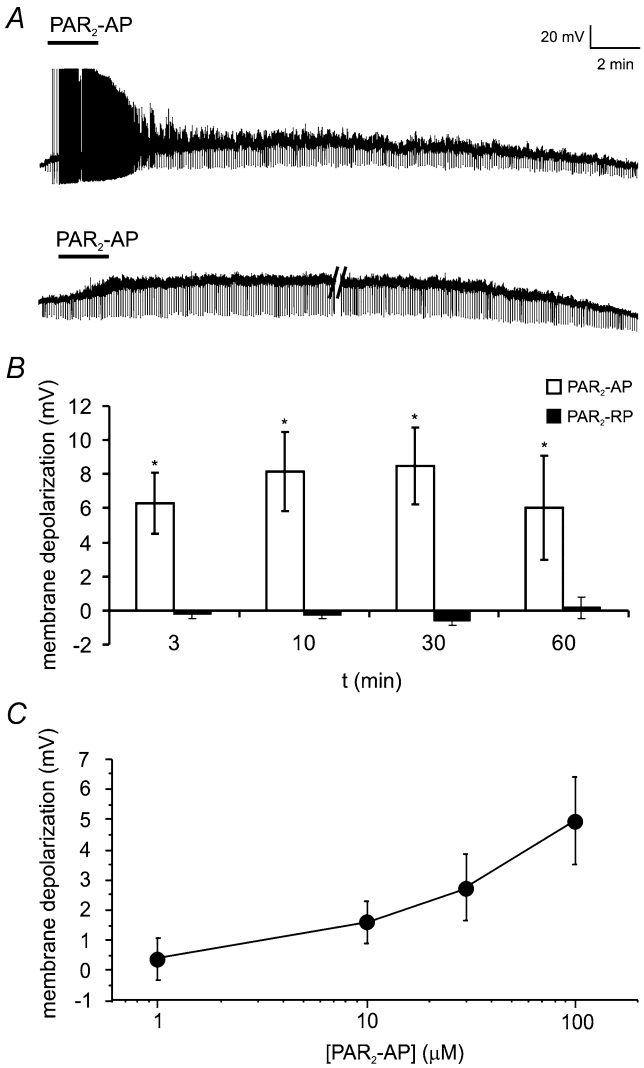

Figure 2. PAR_2-AP evokes sustained depolarization of mouse colonic DRG neurons
A, representative traces showing PAR_2-AP (SLIGRL; 100 μM) superfusion for 3 min caused a sustained depolarization of mouse DRG neurons for up to 60 min. This was associated with action potential discharge in a few neurons (upper trace) and an increase in input resistance (brief downward deflections evoked by constant hyperpolarizing pulse). Parallel lines (lower trace) represent 16 min break in recording. Each neuron was recorded for 5 min prior to application of the PAR_2-AP (not shown) to ensure a stable resting membrane potential. *B*, summary of mean depolarization at each time point following superfusion of PAR_2-AP (100 μM). The reverse peptide, which lacks biological activity at the PAR_2 (PAR_2-RP, LRGILS; 100 μM), had no effect on membrane potential. $n = 5$ or more for each time point. *C*, PAR_2-AP (1–100 μM) evoked a dose-dependent depolarization. $n = 5$ or more neurons at each point.

Effect of PAR_2 activation on K^+ and Na^+ currents

Numerous studies, including our own (Stewart *et al.* 2003; Beyak & Vanner, 2005), have shown that intestinal inflammation and specific inflammatory mediators causes a significant increase in TTX-resistant Na^+ currents

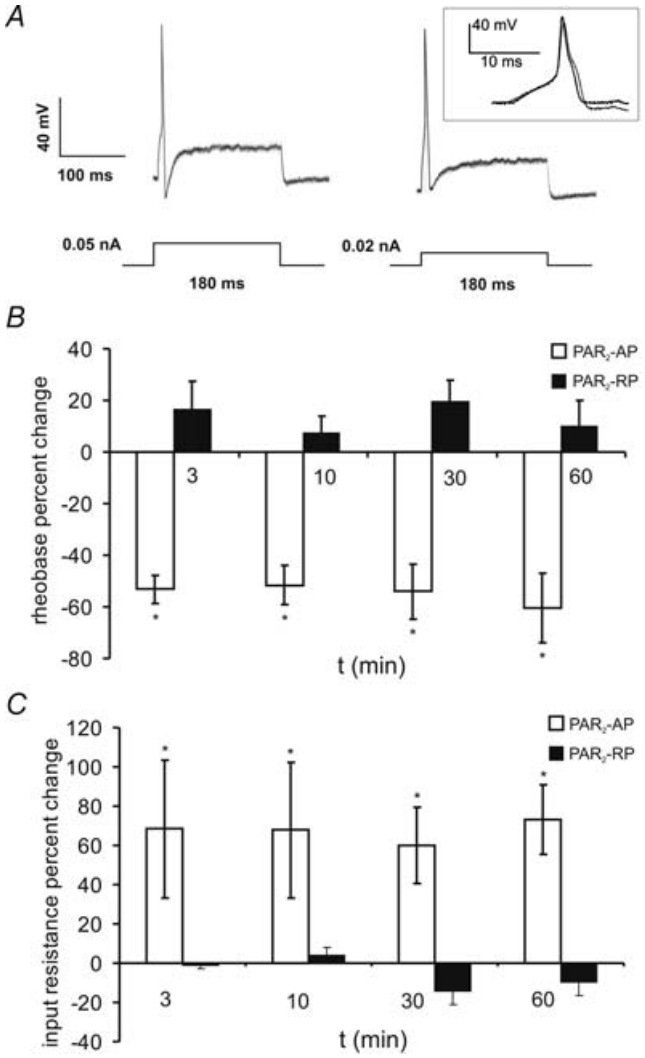

Figure 3. PAR_2-AP-evoked sustained hyperexcitability of mouse colonic DRG neurons
A, representative recording showing rheobase was markedly reduced 10 min (right trace) following a 3 min superfusion of PAR_2-AP (100 μM) compared to time 0 (left trace). The membrane potential was returned to the resting value by injecting depolarizing current at each time point before testing for changes in rheobase. Inset shows that the action potential duration was increased following PAR_2 activation. Rheobase was determined using a series of 0.01 current steps (not shown) and recording the current necessary to elicit an action potential. *B*, summary of percentage decrease in rheobase over time showing change was sustained up to 60 min. In contrast, the PAR_2-RP has no effect. $n = 5$ Fast Blue-labelled neurons at each time point. $^*P < 0.05$ *C*, summary of mean changes in input resistance at each time point showing sustained increase in input resistance. PAR_2-RP had no effect. $n = 5$ Fast Blue-labelled neurons at each time point. $^*P < 0.05$.

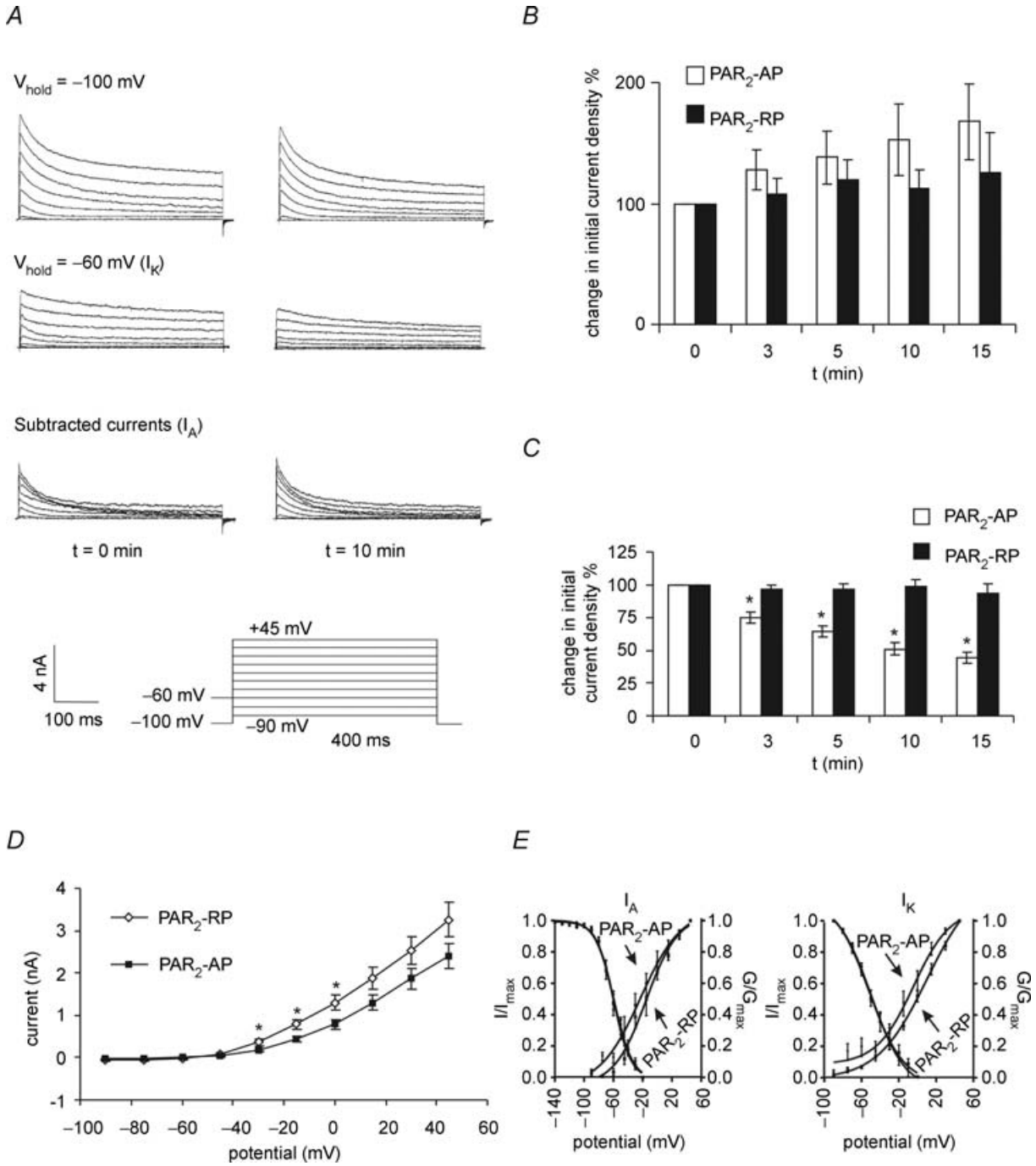

Figure 4. PAR_2 activation suppressed I_K currents
A, representative recordings of transient (I_A) and sustained (I_K) K^+ currents before (left traces) and 10 min following the application of PAR_2-AP (100 μM) (right traces). Currents were measured in voltage clamp from a holding membrane potential of −100 mV or −60 mV using 400 ms steps of 15 mV from −90 mV to +45 mV. I_A was measured by subtracting recordings obtained at a holding membrane potential of −60 mV from recordings obtained at a holding membrane potential of −100 mV. I_A was measured as the peak current in the subtracted recordings. I_K was measured from the trace obtained at a holding membrane potential of −60 mV at $t = 400$ ms. *B* and *C*, summary of the mean current densities following PAR_2 activation for I_A and I_K, respectively. I_A peak current density was not altered, but the I_K peak current density was suppressed. Neurons were superfused for 3 min with PAR_2-AP ($n = 7$) or PAR_2-RP ($n = 8$) (100 μM). $^*P < 0.05$. *D*, current–voltage relationship for delayed rectifier I_K current showing onset of the PAR_2 effect at ∼−45 mV $^*P < 0.05$. *E*, PAR_2-AP did not significantly alter I_A or I_K activation (G/G_{max}) or inactivation kinetics (I/I_{max}). Activation curves for I_A and I_K were measured using 5 mV steps from −80 to +50 mV, and for TTX-R sodium currents from −80 to +10 mV. Normalized conductance

Table 1. The effect of PAR2 activation on V_{50} and *k*-values

	PAR2-AP		PAR2-RP	
Experiment	V_{50} (mV)	*k*	V_{50} (mV)	*k*
I_A				
Activation	-22.7 ± 6.8	27.9 ± 9.2	-15.2 ± 4.4	21.8 ± 4.9
Inactivation	-59.2 ± 1.5	-12.7 ± 1.3	-59.6 ± 1.7	-11.9 ± 1.4
I_K				
Activation	-4.3 ± 5.2	19.8 ± 4.9	10.1 ± 5.4	26.6 ± 3.8
Inactivation	-49.7 ± 2.8	-18.2 ± 3.6	-52.1 ± 3.4	-18.5 ± 4.0
TTX-R Na_v				
Activation	-43.4 ± 1.2	3.8 ± 1.0	-41.5 ± 1.0	3.9 ± 0.8
Inactivation	-29.9 ± 1.5	-5.7 ± 1.3	-31.3 ± 0.5	-5.3 ± 0.4

PAR_2 activation did not alter voltage of half-activation/inactivation (V_{50}) or the slope (*k*) in I_A, I_K, or TTX-resistant Na^+ currents.

($Na_v1.8$) and/or a suppression of transient I_A, and/or delayed rectifier I_K potassium currents. We therefore examined whether changes in these currents may underlie the effects of PAR_2 activation on neuronal excitability.

***I_A* and *I_K* currents.** In the whole-cell voltage-clamp mode we observed a frequent run-down in K^+ membrane currents over a 5–10 min period. Preliminary studies using the perforated-patch-clamp mode demonstrated that, unlike in whole-cell mode, current run-down did not occur in perforated control neurons over the 15 min time period studied. The transient I_A current was blocked by 4-aminopyridine (1 mM; $n = 3$), as previously described (Stewart *et al.* 2003).

Using the perforated-patch technique, superfusion of PAR_2-AP (100 μM) ($n = 7$, 3 Fast Blue-labelled, 4 unlabelled neurons) caused a significant decrease in I_K at 3 min (mean = 23.7%; $P < 0.05$) (Fig. 4). This persisted for the duration of the recording period and was maximal by 10 min (mean = 51.5%). No differences were observed between Fast Blue-labelled and non-labelled neurons. In contrast, PAR_2 activation had no effect on I_A currents (Fig. 4). Similarly, superfusion of PAR_2-RP (100 μM) had no effect on I_A or I_K (Fig. 4). Correlation of the current–voltage relationship (Fig. 4*D*) for I_K demonstrated PAR_2 significantly decreased currents near -40 mV, suggesting this effect was active in the physiological range of membrane potentials.

Voltage-dependence of activation and inactivation (see Methods) were compared, to determine if changes in these parameters could contribute to the reduced current density observed following PAR_2 activation. There were no significant differences in the activation curves for the I_A or I_K currents following superfusion of PAR_2-AP (100 μM; $t = 10$ min) ($n = 7$ for activation curves, 3 Fast Blue-labelled cells) or reverse peptide (100 μM) ($n = 8$, 3 Fast Blue-labelled cells). We also found no significant difference in I_A, or I_K inactivation curves (Fig. 4) between cells superfused with PAR_2-AP (100 μM) (I_A and I_K $n = 5$, unlabelled cells) and PAR_2-RP. The voltage of half-activation and inactivation (V_{50}) and corresponding slope factors (*k*) were determined from the mean of the individual curve fits and are summarized in Table 1. No significant difference was found between the PAR_2-AP and corresponding PAR_2-RP values for V_{50} and *k*.

TTX-resistant Na^+ currents ($Na_v1.8$). TTX-resistant Na^+ currents were obtained using whole-cell recording techniques. In TTX (1 $\mu\mu$), superfusion of cells with PAR_2-AP (100 μM) for 3 min had no effect on TTX-resistant Na^+ currents (Fig. 5; $n = 5$ Fast Blue-labelled cells). Similarly, currents were not altered by the reverse peptide (100 μM) ($n = 4$, 3 Fast Blue-labelled cells). The time course of these currents was similar to those described for slow-inactivating $Na_v1.8$ currents as apposed to ultra-slow-inactivating $Na_v1.9$ currents (Beyak *et al.* 2004). Previous studies have shown that ATP enhances TTX-resistant Na^+ currents in rat DRG neurons (Park *et al.* 2004). Therefore, we also examined whether ATP alters these currents in mouse DRG neurons. When ATP (1 μM) was superfused for 3 min, TTX-resistant Na^+ currents were significantly increased by 3 min following the drug application (285.5%; $n = 3$ Fast Blue-labelled cells; Fig. 5). Further

(G/G_{max}) was plotted against test pulse voltage and fitted to a Boltzmann function. While the activation curves for PAR_2-AP and PAR_2-RP do not overlap, the differences at the various voltage steps are not statistically significant. I_A inactivation curves were generated using a two-pulse protocol: a 1 s prepulse varying between -120 and 0 mV, followed by a 400 ms test pulse of +50 mV. I_K inactivation curves were generated using a two-pulse protocol: an 8 s prepulse varying between -80 and 0 mV followed by a 1 s test pulse of +50 mV.

studies were also conducted using perforated-patch-clamp mode to provide an additional measure that effects of PAR_2 activation were not masked in the whole-cell mode. Using the perforated-patch technique, mean TTX-resistant Na^+ currents were not altered by PAR_2 activation (0 min mean = 2374.2 ± 148.9 pA *versus* 10 min 1797.1 ± 352.0 pA).

Activation curves for TTX-resistant Na^+ currents were not altered (Fig. 5) by prior application of PAR_2-AP (100 μM; $n = 5$, Fast Blue-labelled) compared to cells superfused with PAR_2-RP (100 μM) ($n = 4$, 3 Fast Blue-labelled cells). Similarly, inactivation curves were not altered (Fig. 5) (PAR_2-AP; $n = 3$, all Fast Blue-labelled; PAR_2-RP; $n = 4$, all Fast Blue-labelled). No significant differences were observed between V_{50} and k values obtained with PAR_2-AP compared to PAR_2-RP (Table 1). The threshold for activation of these $Na_v1.8$ currents is more hyperpolarized than that described for other species, as previously reported (Beyak *et al.* 2004).

PAR_2 activation of PKC and $ERK_{1/2}$

$ERK_{1/2}$ and PKC antagonists block PAR_2-induced neuronal excitability. To investigate whether the observed changes in DRG neuronal excitability were mediated by the activation of PKC and $ERK_{1/2}$-dependent pathways, the effects of the PKC inhibitor calphostin C (1 μM) and the $ERK_{1/2}$ inhibitor PD98059 (100 μM) were studied. Calphostin C and PD98059 were added to the intracellular pipette solution and superfused in the extracellular medium during electrophysiological recordings. Neurons were also incubated in PD98059 for 3 h prior to recordings.

Neurons were superfused for 3 min with the PAR_2-AP (100 μM) or PAR_2-RP (100 μM), and recordings were made at 3 and 10 min (Fig. 6). In the presence of either calphostin C ($n = 5$) or PD98059 ($n = 5$), superfusion of PAR_2-AP had no effect on resting membrane potential, rheobase, or input resistance. These measurements of the membrane properties following PAR_2 activation (i.e. in the presence of inhibitors) did not differ from those obtained following the superfusion of the reverse peptide (100 μM) alone ($P > 0.05$), implying that the effects of PAR_2 proceed down PKC and $ERK_{1/2}$-mediated pathways.

To examine the selectivity of PD98059 in DRG neurons, the PKA activator forskolin (1 μM) was studied to determine if PKA-mediated depolarizations were altered by the $ERK_{1/2}$ inhibitor PD98059 (Fig. 6). In these studies forskolin (1 μM) was superfused for 3 min, and changes in membrane potential were recorded at 3 and 10 min. Forskolin depolarized these neurons ($n = 3$, 2 Fast Blue-labelled) at $t = 3$ min (mean = 6.7 mV) and 10 min (mean = 6.7 mV). In separate cells, when forskolin was applied in the presence of PD98059 (100 μM; $n = 3$, 2 Fast Blue-labelled neurons), depolarizations were not substantively different (mean = 6.3 mV at $t = 3$ min, mean = 6.3 mV at $t = 10$ min) compared to those obtained with forskolin alone.

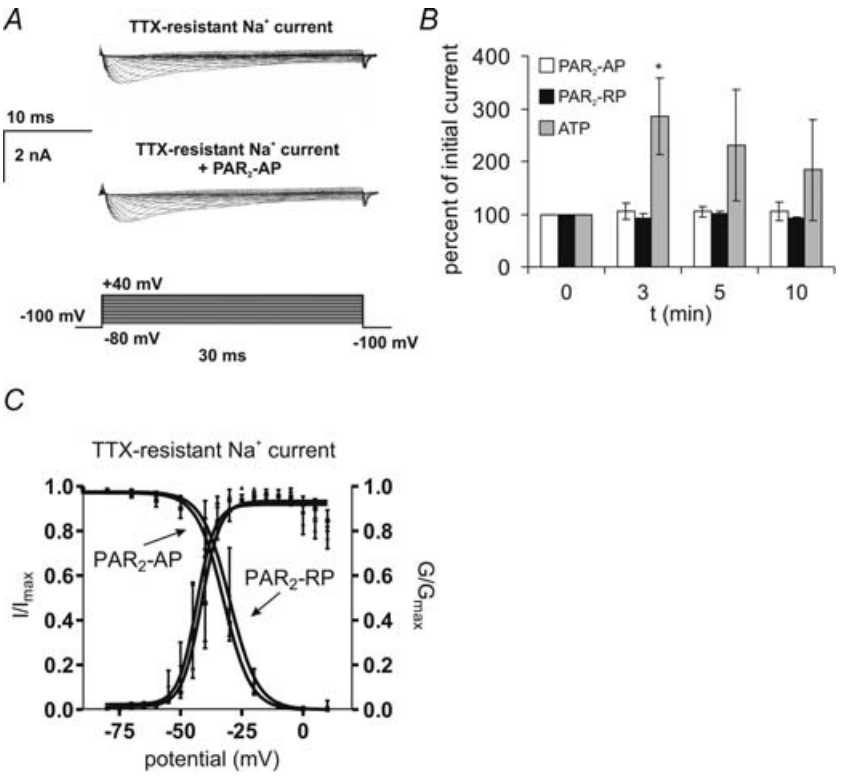

Figure 5. The effect of PAR_2 activation on DRG TTX-R sodium currents
PAR_2 activation did not alter TTX-resistant sodium currents (TTX-R) in DRG neurons. *A*, representative Na^+ currents elicited using 30 ms steps from −80 to +40 mV. TTX-resistant Na^+ currents were isolated with tetrodotoxin (TTX; 1 μM) applied for 3 min. PAR_2-AP (100 μM) was superfused for 3 min and recordings obtained at $t = 3$, 5 and 10 min. PAR_2-AP had no effect on TTX-R Na^+ currents. *B*, summary of change in peak Na^+ current evoked by application of PAR_2-AP ($n = 5$) or PAR_2-RP ($n = 4$). Using the protocol in *A*, cells were also superfused with ATP (1 μM; $n = 3$). ATP caused a significant increase in TTX-R Na^+ currents. $^*P < 0.05$, two-way repeated ANOVA followed by Bonferroni post tests. *C*, PAR_2-AP had no effect on TTX-R-Na^+ activation and inactivation kinetics. TTX-R Na^+ current inactivation curves were generated using a two-pulse protocol, with a 1 s prepulse between −120 and 0 mV, followed by a 30 ms test pulse to 0 mV. Normalized current (I/I_{max}) was plotted against prepulse voltage and fitted to a negative Boltzmann function.

PAR$_2$ agonists activate ERK$_{1/2}$ and induce phosphorylation of ERK$_{1/2}$ at the plasma membrane. We have previously reported that PAR$_2$ agonists activate ERK$_{1/2}$ in transfected cell lines and in enterocytes that naturally express this receptor (Defea *et al.* 2000). Since ERK$_{1/2}$ can phosphorylate and inhibit K_v4.2 in the CNS and thereby enhance neuronal excitability (Adams *et al.* 2000), we determined if PAR$_2$ agonists phosphorylate and thus activate ERK$_{1/2}$ in cultured DRG neurons. In mouse DRG neurons, there were low levels of immunoreactive pERK$_{1/2}$ in the unstimulated state (Fig. 7). When neurons were incubated with PMA (1 μM, 5 min), as a positive control for ERK$_{1/2}$ activation, pERK$_{1/2}$ was observed in the cytosol of neurons, with the most intense signals in close proximity to the plasma membrane (Fig. 7*B*). Incubation of neurons with PAR$_2$-RP (100 μM, 1–15 min), a control agonist that does not activate PAR$_2$, had no effect on levels of detectable pERK$_{1/2}$ (Fig. 7*C*). However, when neurons were incubated with PAR$_2$-AP (100 μM, 1–15 min), pERK$_{1/2}$ was detected in the cytosol of many neurons. PAR$_2$-AP induced the appearance of pERK$_{1/2}$ within 1–5 min (not shown), and by 15 min there were strong signals in the cytosol in close proximity to the

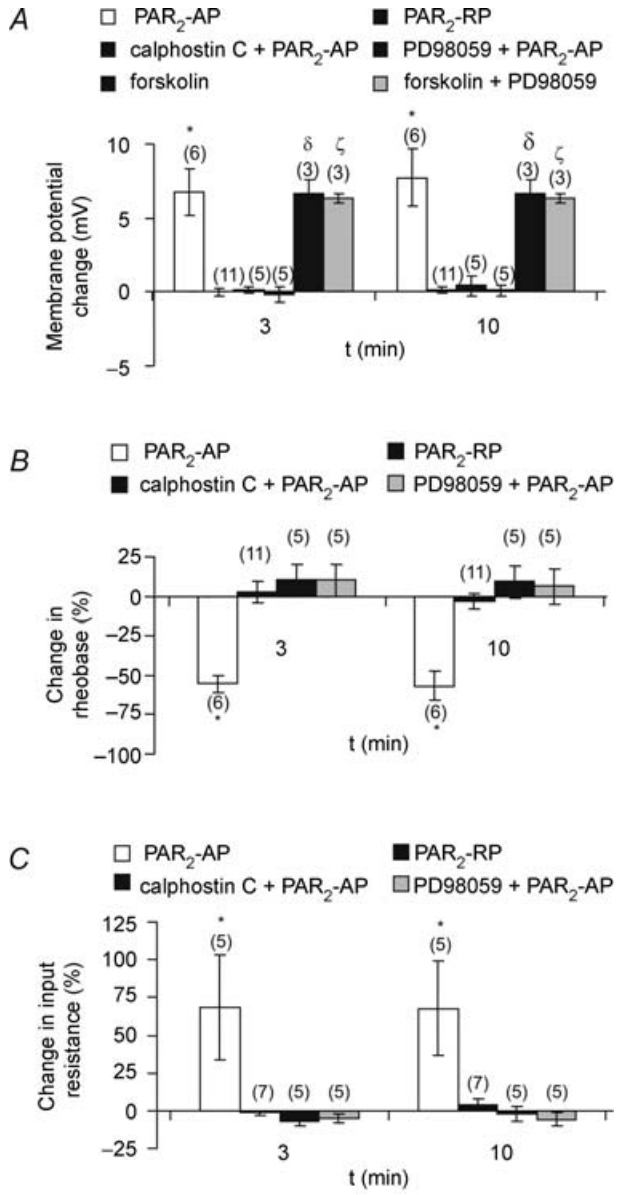

Figure 6. Calphostin C and PD98059 blocked PAR$_2$-evoked DRG neuronal hyperexcitability
A, summary of mean changes in membrane potential evoked by PAR$_2$-AP at 3 and 10 min either alone or in presence of PKC inhibitor calphostin C (1 μM; applied for 3 min by superfusion and in pipette) or the ERK$_{1/2}$ inhibitor PD98059 (100 μM, applied for 3 h to cultures prior to application of PAR$_2$-AP and in pipette). Depolarizations evoked by the PKA agonist forskolin (1 μM) were not inhibited by PK98059, supporting a selective action of this antagonist. *B*, summary of effects of inhibitors on rheobase. *C*, summary of effects on input resistance. For experimental protocol see Figs 2 and 3. The numbers in parentheses indicate the number of cells for every experiment. *, δ and ζ indicate $P < 0.05$ *versus* the PAR$_2$-RP; two-way repeated ANOVA followed by Bonferroni post tests.

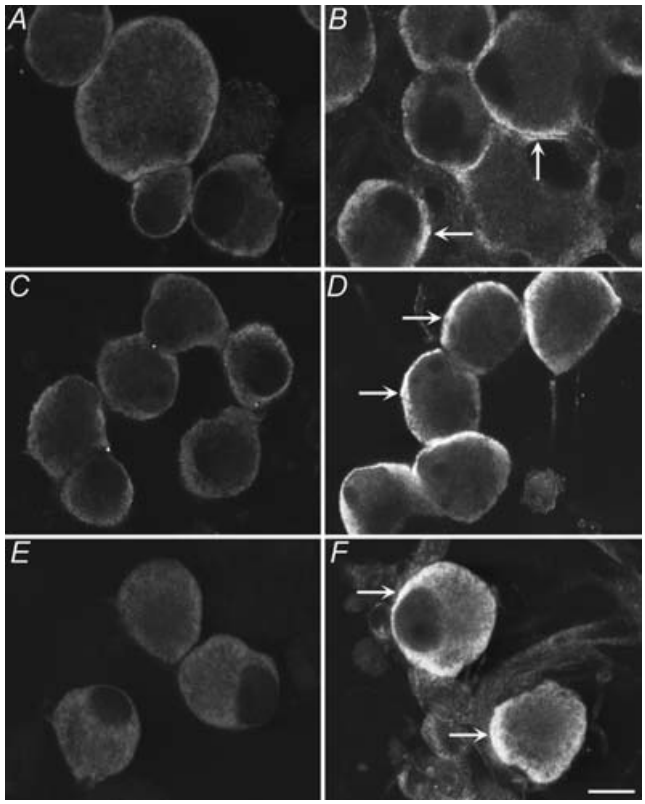

Figure 7. Localization of pERK$_{1/2}$ in cultured DRG neurons from mice (*A*–*D*) and rats (*E* and *F*)
A, unstimulated neurons; *B*, PMA, 1 μM, 5 min; *C*, PAR$_2$-RP, 100 μM, 15 min; *D*, PAR$_2$-AP, 100 μM, 15 min; *E*, unstimulated neurons; *F*, PAR$_2$-AP (100 μM, 15 min). When neurons were incubated with PMA or PAR$_2$-AP, pERK$_{1/2}$ were detected in the cytosol in close proximity to the plasma membrane (arrows), whereas PAR$_2$-RP (control) had no effect on the levels of pERK$_{1/2}$. Representative images are shown from experiments with neurons prepared from $n > 3$ animals. Scale bar = 20 μm.

plasma membrane (Fig. 7*D*). Since we have previously reported that PAR_2 activators cause hyperexcitability of DRG neurons in rats, we also determined if they activate $ERK_{1/2}$ in DRG neurons from this species. There were low levels of detectable immunoreactive $pERK_{1/2}$ in unstimulated rat DRG neurons (Fig. 7*E*). When neurons were incubated with PMA (1 μM) or PAR_2-AP (100 μM) for 1–15 min, $pERK_{1/2}$ was detected in the cytosol of many neurons in close proximity to the plasma membrane (PMA, not shown, PAR_2-AP 15 min, Fig. 7*F*). As a control, PAR_2-RP had no effect on levels of $pERK_{1/2}$ in rat DRG neurons (not shown). Together, these results suggest that PAR_2 agonists stimulate activation of $ERK_{1/2}$ in the region of the plasma membrane, where $ERK_{1/2}$ may phosphorylate and thereby control the activity of ion channels that regulate neuronal excitability.

Discussion

This study demonstrates that PAR_2 agonists applied to neurons from mouse DRG caused a remarkably sustained hyperexcitability of these neurons. Several steps were taken to further clarify the relevance of this finding. Firstly, small neurons were targeted in these studies because they express properties associated with nociceptors (i.e. TTX-resistant action potentials, TRPV1 receptors, substance P and CGCP immunoreactivity) (Gold *et al.* 1996*a*; Yoshimura & de Groat, 1999; Moore *et al.* 2002; Stewart *et al.* 2003; Beyak *et al.* 2004; Beyak & Vanner, 2005). Secondly, electrophysiological recordings were obtained in neurons labelled with retrograde tracers injected into the wall of the colon, confirming that these findings were characteristic of nociceptors innervating the colon. Finally, we also demonstrated that labelled neurons from the colon expressed PAR_2 immunoreactivity. Together, these findings demonstrate that activation of PAR_2 on the plasma membrane of nociceptive DRG neurons innervating the mouse colon leads to sustained hyperexcitability.

Sustained neuronal hyperexcitability

The long-lasting changes in membrane potential and rheobase observed in this study lasted up to 1 h after a brief application of the PAR_2 agonist. We have observed similar sustained effects on enteric neurons (Reed *et al.* 2003) and other studies of unidentified rat DRG neurons (Amadesi *et al.* 2004). The specificity of the PAR_2 agonists used in the current study has been carefully demonstrated in our previous studies (Reed *et al.* 2003; Amadesi *et al.* 2004) and others (Nystedt *et al.* 1994; Dai *et al.* 2004). Consistent with these observations, in the present study we found that PAR_2-AP had a dose-dependent effect, which was mimicked by trypsin, whereas the reverse peptide, which lacks biological activity at PAR_2, had no effect. This specificity has also been observed in studies demonstrating that PAR_2-AP directly activates intestinal afferents in anaesthetized animals (Kirkup *et al.* 2003).

Ionic mechanism(s) underlying sustained hyperexcitability

There is considerable evidence that voltage-gated Na^+ and K^+ channels underlying action potential electrogenesis are modulated by visceral inflammation or specific inflammatory mediators (Gold *et al.* 1996*a*; Yoshimura & de Groat, 1999; Gebhart *et al.* 2002; Beyak *et al.* 2004; Dang *et al.* 2004; Beyak & Vanner, 2005). The most common findings are that TTX-resistant Na^+ currents ($Na_v1.8$) are increased and/or voltage-gated K^+ currents, namely I_A and I_K, are suppressed. However, the specific channel(s) affected may be dependent on the nature of the inflammation (Beyak & Vanner, 2005*c*) and/or the inflammatory mediator.

In the current study, mouse colonic DRG neurons exhibited transient I_A and sustained delayed-rectifier I_K voltage-gated K^+ currents (see Fig. 4) characteristic of other DRG neurons (McFarlane & Cooper, 1991; Stewart *et al.* 2003; Dang *et al.* 2004; Beyak & Vanner, 2005). The voltage and 4-AP sensitivity (Stewart *et al.* 2003) of the transient K^+ currents were typical of I_A currents, and the kinetics of the I_K currents match those described in other species (Stewart *et al.* 2003; Dang *et al.* 2004). We found that the hyperexcitability following PAR_2 activation was associated with a profound suppression of the I_K currents (>50%) but not of I_A. The effect was active in the physiological range of membrane potentials (Fig. 4) (i.e. around the threshold for action potential electrogenesis), and therefore may contribute to the decrease in rheobase observed with PAR_2 activation. However, models of visceral inflammation in the ileum, stomach and bladder (Yoshimura & de Groat, 1999; Stewart *et al.* 2003;Dang *et al.* 2004) have also shown that I_A is suppressed in models of chronic inflammation, supporting the notion that individual mediators may signal preferentially to selective K^+ channels. Previous studies of the biophysical and pharmacological properties of I_K currents suggest these currents may comprise three distinct currents (Gold *et al.* 1996*b*). The molecular determinants of the channels underlying these I_K currents are currently unknown although studies suggest candidates of the α-subunits include K_V 2.1/2.2 and 3.1/3.2 (Song, 2002; Kim *et al.* 2002).

In addition to the observed changes in I_K currents, our findings also suggest that PAR_2 activation affects other K^+ currents. The increases in membrane depolarization and input resistance following PAR_2 activation cannot be accounted for by I_K currents, because they were not open at the resting membrane potential. It is probable that these changes result from closure of background or 'leak' K^+-selective channels. These channels may be members

of the two, and possibly four, transmembrane segment K^+ channels (Patel & Honore, 2001), which are important targets of neurotransmitters and paracrine agents.

An array of inflammatory mediators including adenosine, 5-HT, ATP, PGE_2 and NGF have been found to enhance TTX-resistant Na^+ currents ($Na_v1.8$) in nociceptive DRG neurons (Gold *et al.* 1996*a*; Cardenas *et al.* 2001; Zhang *et al.* 2002; Park *et al.* 2004; Beyak & Vanner, 2005). In models of established inflammation in the stomach, ileum, colon, and bladder (Yoshimura & de Groat, 1999; Gebhart *et al.* 2002; Stewart *et al.* 2003; Beyak *et al.* 2004) these currents were also found to be increased in neurons innervating the inflamed segments. Somewhat surprisingly, in our study PAR_2 activation had no effect on this current. To demonstrate we could induce current increases in our neurons, we also tested ATP and found that this mediator enhanced currents, as predicted by other studies (Park *et al.* 2004). Recent studies have also suggested TTX-sensitive Na^+ currents ($Na_v1.7$) may also be modulated by inflammation (Black *et al.* 2004). We cannot conclude that PAR_2 activation does not modulate these currents because they were not examined in our study. However, this seems unlikely given that previous studies examining the effects of inflammation either failed to observe an effect on TTX-sensitive Na^+ current (Yoshimura & de Groat, 1999; Gebhart *et al.* 2002; Beyak *et al.* 2004) or, in the recent study, suggested an effect on TTX-sensitive Na^+ currents (Black *et al.* 2004), which paralleled the effects on TTX-resistant Na^+ currents. We also did not examine the possibility that TTX-resistant $Na_v1.9$ currents were modulated by PAR_2 activation. However our previous studies (Beyak *et al.* 2004) suggest these currents are not frequently found in nociceptive DRG neurons innervating the mouse colon, and furthermore other studies suggest that measurement of pharmacological effects on these currents can be extremely difficult (Maruyama *et al.* 2004). Finally, although our findings strongly suggest that PAR_2 activation does not directly modulate $Na_v1.8$ currents, this may occur through indirect mechanisms in the whole animal because PAR_2 stimulates PGE_2 and CGRP release from nerve terminals (Steinhoff *et al.* 2000; Vergnolle *et al.* 2003) and these agents in turn can enhance the Na^+ currents (Baker, 2005; Natura *et al.* 2005).

PAR_2 signal transduction mechanisms of hyperexcitability in colonic DRG neurons

The intracellular mechanism(s) that underlie the sustained hyperexcitability evoked by PAR_2 activation on DRG neurons described in this study and others is unknown. Our findings suggest $ERK_{1/2}$ signalling may play a major role because PAR_2 activation stimulates phosphorylation of $ERK_{1/2}$ at the plasma membrane (Fig. 7) where it could modulate ion channels, and the highly selective $ERK_{1/2}$ inhibitor (PD98059) (Thomas & Huganir, 2004) blocked the PAR_2-mediated effects on neuronal excitability (Fig. 6). We were specifically interested in examining the potential role of $ERK_{1/2}$ signalling because recent reports in the CNS (Thomas & Huganir, 2004) suggest that $ERK_{1/2}$ signals not only to nuclear pathways regulating gene expression but also to cytoplasmic proteins including voltage-gated K^+ channels. Moreover, phosphorylation of these channels in an ERK-dependent manner in the hippocampus underlies some forms of sustained excitability. Several recent studies have also demonstrated activation of $ERK_{1/2}$ in peripheral DRG neurons (Seino *et al.* 2006; Takahashi *et al.* 2006).

The signal transduction pathway by which PAR_2 agonists activate $ERK_{1/2}$ in neurons also remains to be defined. However, possible mechanisms include the trans-activation of growth factor receptors, activation of protein kinase C, and β-arrestin-dependent activation (Defea *et al.* 2000; Darmoul *et al.* 2004). We did observe that calphostin, a PKC blocker, also inhibited the PAR_2-induced neuronal hyperexcitability (see Fig. 6), but further studies are needed to examine the interaction of PKC and $ERK_{1/2}$. β-arrestin-dependent mechanisms may be of particular importance in targeting activated $EERK_{1/2}$ to the plasma membrane, where they may phosphorylate and regulate ion channels (Defea *et al.* 2000; Luttrell & Lefkowitz, 2002). Agonists of many G-protein-coupled receptors, including PAR_2, stimulate the translocation of β-arrestins from the cytosol to phosphorylate receptors at the plasma membrane (Dery *et al.* 1999; Luttrell & Lefkowitz, 2002). β-Arrestins act to uncouple receptors from heterotrimeric G-proteins and thereby desensitize G-protein signalling, couple G-protein-coupled receptors to clathrin and AP_2, and thereby mediate receptor endocytosis. β-Arrestins are also molecular scaffolds that recruit and organize components of the MAP kinase pathway to activated G-protein-coupled receptors, thereby determining the subcellular location and function of activated $ERK_{1/2}$. We have shown that agonists of PAR_2 promote the assembly of a stable signalling complex in cells that includes PAR_2, β-arrestins, raf-1, MEKK and $pERK_{1/2}$ (Defea *et al.* 2000). This complex acts to prevent the trafficking of activated $ERK_{1/2}$ to the nucleus and instead retain $ERK_{1/2}$ within the cytosol, where it could phosphorylate and regulate other targets, including ion channels. Whether this mechanism occurs in neurons and permits $ERK_{1/2}$ to regulate ion channels that mediate PAR_2-induced hyperexcitability, such as those underlying I_K currents, remains to be determined.

Implications of PAR_2-evoked sustained hyperexcitability of nociceptive DRG neurons in the colon

There is growing evidence that the release of proteases from mast cells plays an important role in the genesis of

visceral hyperalgesia in functional bowel disorders such as IBS (Barbara *et al.* 2004; Spiller & Campbell, 2006; Barbara *et al.* 2006). Studies have demonstrated that intestinal mast cell numbers are increased, at least in subsets of patients, and that there is evidence of increased degranulation and tissue content of mast cell tryptase. Moreover, preliminary studies have shown that tryptase in the supernatant of colonic biopsies from IBS patients can stimulate calcium signals in DRG neurons (Cenac *et al.* 2005), suggesting activation of these neurons. The proximity of mast cells to nerve terminals in the intestine has also been correlated with the severity of abdominal pain (Barbara *et al.* 2004). Numerous *in vitro* and *in vivo* animal studies have also shown that proteases, such as tryptase, released from degranulating mast cells have similar actions to those induced by the PAR_2 agonists used in this study. When taken together, the findings of the current study combined with these previous studies suggest it is possible that the sustained excitability of nociceptive DRG neurons following PAR_2 activation could be important in the genesis of abdominal pain in patients with IBS, and that repeated mast cell degranulation may lead to ongoing 're-priming' of these neurons.

References

Adams JP, Anderson AE, Varga AW, Dineley KT, Cook RG, Pfaffinger PJ & Sweatt JD (2000). The A-type potassium channel Kv4.2 is a substrate for the mitogen-activated protein kinase ERK. *J Neurochem* **75**, 2277–2287.

Amadesi S, Nie J, Vergnolle N, Cottrell GS, Grady EF, Trevisani M, Manni C, Geppetti P, McRoberts JA, Ennes H, Davis JB, Mayer EA & Bunnett NW (2004). Protease-activated receptor 2 sensitizes the capsaicin receptor transient receptor potential vanilloid receptor 1 to induce hyperalgesia. *J Neurosci* **24**, 4300–4312.

Baker MD (2005). Protein kinase C mediates up-regulation of tetrodotoxin-resistant, persistent Na^+ current in rat and mouse sensory neurones. *J Physiol* **567**, 851–867.

Barbara G, De Stanghellini V, GR & Corinaldesi R (2006). Functional gastrointestinal disorders and mast cells: implications for therapy. *Neurogastroenterol Motil* **18**, 6–17.

Barbara G, De Stanghellini VGR, Cremon C, Cottrell GS, Santini D, Pasquinelli G, Morselli-Labate AM, Grady EF, Bunnett NW, Collins SM & Corinaldesi R (2004). Activated mast cells in proximity to colonic nerves correlate with abdominal pain in irritable bowel syndrome. *Gastroenterology* **126**, 693–702.

Beyak MJ, Ramji N, Krol KM, Kawaja MD & Vanner SJ (2004). Two TTX-resistant Na^+ currents in mouse colonic dorsal root ganglia neurons and their role in colitis-induced hyperexcitability. *Am J Physiol Gastrointest Liver Physiol* **287**, G845–G855.

Beyak MJ & Vanner S (2005). Inflammation-induced hyperexcitability of nociceptive gastrointestinal DRG neurones: the role of voltage-gated ion channels. *Neurogastroenterol Motil* **17**, 175–186.

Black JA, Liu S, Tanaka M, Cummins TR & Waxman SG (2004). Changes in the expression of tetrodotoxin-sensitive sodium channels within dorsal root ganglia neurons in inflammatory pain. *Pain* **108**, 237–247.

Cardenas LM, Cardenas CG & Scroggs RS (2001). 5HT increases excitability of nociceptor-like rat dorsal root ganglion neurons via cAMP-coupled TTX-resistant Na^+ channels. *J Neurophysiol* **86**, 241–248.

Cenac N, Chapman K, Andrade-Gordon P, Ferrez J, Andrews C, Schaffer E & Vergnolle N (2005). Role for proteases and protease-activated receptor-2 (PAR2) in pain associated with irritable bowel syndrome (IBS). *Gastroenterol* **128** (Suppl. 2), P-20.

Dai Y, Moriyama T, Higashi T, Togashi K, Kobayashi K, Yamanaka H, Tominaga M & Noguchi K (2004). Proteinase-activated receptor 2-mediated potentiation of transient receptor potential vanilloid subfamily 1 activity reveals a mechanism for proteinase-induced inflammatory pain. *J Neurosci* **24**, 4293–4299.

Dang K, Bielefeldt K & Gebhart GF (2004). Gastric ulcers reduce A-type potassium currents in rat gastric sensory ganglion neurons. *Am J Physiol Gastrointest Liver Physiol* **286**, G573–G579.

Darmoul D, Gratio V, Devaud H & Laburthe M (2004). Protease-activated receptor 2 in colon cancer: trypsin-induced MAPK phosphorylation and cell proliferation are mediated by epidermal growth factor receptor transactivation. *J Biol Chem* **279**, 20927–20934.

Defea KA, Zalevsky J, Thoma MS, Dery O, Mullins RD & Bunnett NW (2000). beta-arrestin-dependent endocytosis of proteinase-activated receptor 2 is required for intracellular targeting of activated ERK1/2. *J Cell Biol* **148**, 1267–1281.

Dery O, Thoma MS, Wong H, Grady EF & Bunnett NW (1999). Trafficking of proteinase-activated receptor-2 and beta-arrestin-1 tagged with green fluorescent protein. beta-Arrestin-dependent endocytosis of a proteinase receptor. *J Biol Chem* **274**, 18524–18535.

gado-Aros S & Camilleri M (2005). Visceral hypersensitivity. *J Clin Gastroenterol* **39**, S194–S203.

Gebhart GF, Bielefeldt K & Ozaki N (2002). Gastric hyperalgesia and changes in voltage gated sodium channel function in the rat. *Gut* **51** (Suppl. 1), i15–i18.

Gold MS, Reichling DB, Shuster MJ & Levine JD (1996*a*). Hyperalgesic agents increase a tetrodotoxin-resistant Na^+ current in nociceptors. *Proc Natl Acad Sci U S A* **93**, 1108–1112.

Gold MS, Shuster MJ & Levine JD (1996*b*). Characterization of six voltage-gated K^+ currents in adult rat sensory neurons. *J Neurophysiol* **75**, 2629–2646.

Kim DS, Choi JO, Rim HD & Cho HJ (2002). Downregulation of voltage-gated potassium channel alpha gene expression in dorsal root ganglia following chronic constriction injury of the rat sciatic nerve. *Brain Res Mol Brain Res* **105**, 146–152.

Kirkup AJ, Jiang W, Bunnett NW & Grundy D (2003). Stimulation of proteinase-activated receptor 2 excites jejunal afferent nerves in anaesthetised rats. *J Physiol* **552**, 589–601.

Lembo A, Ameen VZ & Drossman DA (2005). Irritable bowel syndrome: toward an understanding of severity. *Clin Gastroenterol Hepatol* **3**, 717–725.

Lomax AE, O'Hara JR, Hyland NP, Mawe GM & Sharkey KA (2006). Persistent alterations to enteric neural signalling in guinea pig colon following resolution of colitis. Am J Physiol Gastrointest Liver Physiol. *Am J Physiol Gastrointest Liver Physiol* **292**, G482–4891.

Luttrell LM & Lefkowitz RJ (2002). The role of beta-arrestins in the termination and transduction of G-protein-coupled receptor signals. *J Cell Sci* **115**, 455–465.

Maruyama H, Yamamoto M, Matsutomi T, Zheng T, Nakata Y, Wood JN & Ogata N (2004). Electrophysiological characterization of the tetrodotoxin-resistant Na^+ channel, $Na_v1.9$, in mouse dorsal root ganglion neurons. *Pflugers Arch* **449**, 76–87.

Mawe GM, Collins SM & Shea-Donohue T (2004). Changes in enteric neural circuitry and smooth muscle in the inflamed and infected gut. *Neurogastroenterol Motil* **16** (Suppl. 1), 133–136.

McFarlane S & Cooper E (1991). Kinetics and voltage dependence of A-type currents on neonatal rat sensory neurons. *J Neurophysiol* **66**, 1380–1391.

Moore BA, Stewart TM, Hill C & Vanner SJ (2002). TNBS ileitis evokes hyperexcitability and changes in ionic membrane properties of nociceptive DRG neurons. *Am J Physiol Gastrointest Liver Physiol* **282**, G1045–G1051.

Natura G, von Banchet GS & Schaible HG (2005). Calcitonin gene-related peptide enhances TTX-resistant sodium currents in cultured dorsal root ganglion neurons from adult rats. *Pain* **116**, 194–204.

Nystedt S, Emilsson K, Wahlestedt C & Sundelin J (1994). Molecular cloning of a potential proteinase activated receptor. *Proc Natl Acad Sci U S A* **91**, 9208–9212.

Park SY, Kim HI, Shin YK, Lee CS, Park M & Song JH (2004). Modulation of sodium currents in rat sensory neurons by nucleotides. *Brain Res* **1006**, 168–176.

Patel AJ & Honore E (2001). Properties and modulation of mammalian 2P domain K^+ channels. *Trends Neurosci* **24**, 339–346.

Rae J, Cooper K, Gates P & Watsky M (1991). Low access resistance perforated patch recordings using amphotericin B. *J Neurosci Meth* **37**, 15–26.

Reed DE, Barajas-Lopez C, Cottrell G, Velazquez-Rocha S, Dery O, Grady EF, Bunnett NW & Vanner SJ (2003). Mast cell tryptase and proteinase-activated receptor 2 induce hyperexcitability of guinea-pig submucosal neurons. *J Physiol* **547**, 531–542.

Saito T & Bunnett NW (2005). Protease-activated receptors: regulation of neuronal function. *Neuromolecular Med* **7**, 79–99.

Sandler RS, Drossman DA, Nathan HP & McKee DC (1984). Symptom complaints and health care seeking behavior in subjects with bowel dysfunction. *Gastroenterology* **87**, 314–318.

Seino D, Tokunaga A, Tachibana T, Yoshiya S, Dai Y, Obata K, Yamanaka H, Kobayashi K & Noguchi K (2006). The role of ERK signaling and the P2X receptor on mechanical pain evoked by movement of inflamed knee joint. *Pain* **123**, 193–203.

Song WJ (2002). Genes responsible for native depolarization-activated K^+ currents in neurons. *Neurosci Res* **42**, 7–14.

Spiller R & Campbell E (2006). Post-infectious irritable bowel syndrome. *Curr Opin Gastroenterol* **22**, 13–17.

Steinhoff M, Vergnolle N, Young SH, Tognetto M, Amadesi S, Ennes HS, Trevisani M, Hollenberg MD, Wallace JL, Caughey GH, Mitchell SE, Williams LM, Geppetti P, Mayer EA & Bunnett NW (2000). Agonists of proteinase-activated receptor 2 induce inflammation by a neurogenic mechanism. *Nat Med* **6**, 151–158.

Stewart T, Beyak MJ & Vanner S (2003). Ileitis modulates potassium and sodium currents in guinea pig dorsal root ganglia sensory neurons. *J Physiol* **552**, 797–807.

Takahashi N, Kikuchi S, Shubayev VI, Campana WM & Myers RR (2006). TNF-alpha and phosphorylation of ERK in DRG and spinal cord: insights into mechanisms of sciatica. *Spine* **31**, 523–529.

Thomas GM & Huganir RL (2004). MAPK cascade signalling and synaptic plasticity. *Nat Rev Neurosci* **5**, 173–183.

Vergnolle N, Ferazzini M, D'Andrea MR, Buddenkotte J & Steinhoff M (2003). Proteinase-activated receptors: novel signals for peripheral nerves. *Trends Neurosci* **26**, 496–500.

Vergnolle N, Wallace JL, Bunnett NW & Hollenberg MD (2001). Protease-activated receptors in inflammation, neuronal signaling and pain. *Trends Pharmacol Sci* **22**, 146–152.

Yoshimura N & de Groat WC (1999). Increased excitability of afferent neurons innervating rat urinary bladder after chronic bladder inflammation. *J Neurosci* **19**, 4644–4653.

Zhang YH, Vasko MR & Nicol GD (2002). Ceramide, a putative second messenger for nerve growth factor, modulates the TTX-resistant Na^+ current and delayed rectifier K^+ current in rat sensory neurons. *J Physiol* **544**, 385–402.

Acknowledgements

We thank Lorna Divino and Iva Kosatka for excellent technical support. This work was supported by grants from NIH (DK57840 and D43207, NWB), CIHR (SV) and CCFC (SV).